Modeling of detective quantum efficiency considering scatter-reduction devices

Jiwoong Park[a], Dong Woon Kim[a], Ho Kyung Kim[a,b*]
[a]*School of Mechanical Engineering, Pusan National University, Busan, South Korea*
[b]*Center for Advanced Medical Engineering Research, Pusan National University, Busan, South Korea*
[*]*Corresponding author: hokyung@pusan.ac.kr*

1. Introduction

Production of scattered x-ray photons in screening-mammography procedures is inevitable, and the scatter degrades image contrast as if it plays a role of an additional noise source. The reduction of signal-to-noise ratio (SNR) cannot be restored and thus has become a severe issue in digital mammography.[1] Therefore, anti-scatter grids are typically used in mammography.
Scatter-cleanup performance of various scatter-reduction devices, such as air gaps,[2] linear (1D) or cellular (2D) grids,[3, 4] and slot-scanning devices,[5] has been extensively investigated by many research groups. In the present time, a digital mammography system with the slot-scanning geometry is also commercially available.[6]
In this study, we theoretically investigate the effect of scattered photons on the detective quantum efficiency (DQE) performance of digital mammography detectors by using the cascaded-systems analysis (CSA) approach. We show a simple DQE formalism describing digital mammography detector systems equipped with scatter reduction devices by regarding the scattered photons as additive noise sources. Using the developed DQE model, we investigate the effect of scatter-reduction devices on the DQE considering their typical performances of scatter cleanup..

2. Material and Methods

For an incident x-ray fluence $\bar{q}_0$, Fig. 1 shows a series of quantum-interaction processes to produce the mean pixel signal $\bar{d}$ in a digital mammography detector system. The scatter photons are considered by adding them into the incident fluence such that $\bar{q}_0 = \bar{q}_0^P + \bar{q}_0^S$, where the superscripts P and S denote the primary and the scatter, respectively. The fraction of scatter photons in the incident fluence can be quantified by the scatter-to-primary ratio, SPR_0 ($= \bar{q}_0^S/\bar{q}_0^P$). It is assumed that any scatter-reduction device, such as grids, air gaps, or scanning devices, modifies only the SPR_0 so that we designate the photon fluence behind a scatter-reduction device as $\bar{q} = \bar{q}^P + \bar{q}^S$. The performance of a scatter-reduction device may be characterized by the primary and scatter transmission factors: $\tau_P = \bar{q}^P/\bar{q}_0^P$ and $\tau_S = \bar{q}^S/\bar{q}_0^S$. With cascaded system analysis, we develop the system given by

$$\mathrm{DQE}_{sys}(u,v) = \frac{T_{sys}^2(u,v)}{\frac{1}{\mathrm{DQE}_{grid}}\left[\frac{1}{\gamma\alpha\beta\eta}+\frac{T_{sys}^{I2}(u,v)}{\alpha}\left(\frac{1}{I}-\frac{1}{\beta}\right)\right]+\frac{p^2\sigma_{add}^2}{\bar{q}_0^P\tau_P^2\bar{G}^2}}, \quad (1)$$

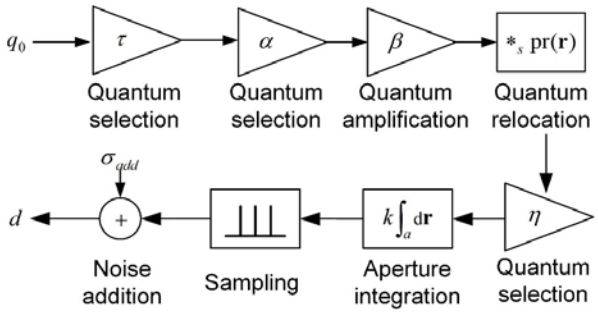

Figure 1. Cascaded-block diagram describing signal and noise propagation in the grid-detector system. The symbol "$*_s$" is the quantum scatter operator.

where $\mathrm{DQE}_{grid} = \frac{\tau_P}{1+\Sigma^{-1}\mathrm{SPR}_0}$, which is the DQE of a scatter-reduction device.

To validate the DQE model derived in this study, we measured the DQE of a complementary metal-oxidesemiconductor (CMOS) flat-panel detector (Shad-o-Box 1548 HS, Teledyne Rad-icon Imaging Corp., Sunnyvale,CA) placed behind the PMMA slabs with thickness range 10-30 mm for the W/Al spectrum of an x-ray tube (Oxford Instruments, Inc., USA) operated at 30 kVp. The detector had a pixel pitch of 0.099 mm and a pixel format of 1548_1032. As an x-ray conversion into optical quanta, the detector used a Gd_2O_2S:Tb phosphor screen. The phosphor was coupled to the CMOS photodiode array through an fiber-optic plate.
The MTF describing an impulse response of an imaging detector in the Fourier domain may be analyzed by a weighted combination of Gaussian and Lorentzian functions:

$$T_{fit}(u) = \omega e^{-p_1 u^2} + \frac{1-\omega}{1+p_2(u+u^2)}, \quad (2)$$

where ω denotes a weight and p_1 and p_2 are fit parameters. If the scatter is included into the MTF

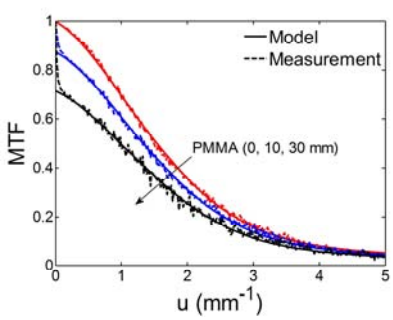

Figure 2. MTF results for various thicknesses of PMMA. The solid lines indicate the fit results with Eqs. 2 and 3.

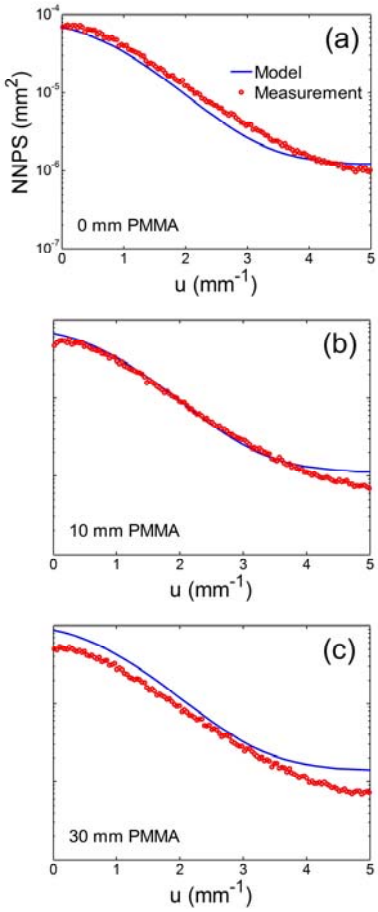

Figure 3. Comparisons of the measured and calculated NNPSs for various amounts of scatter.

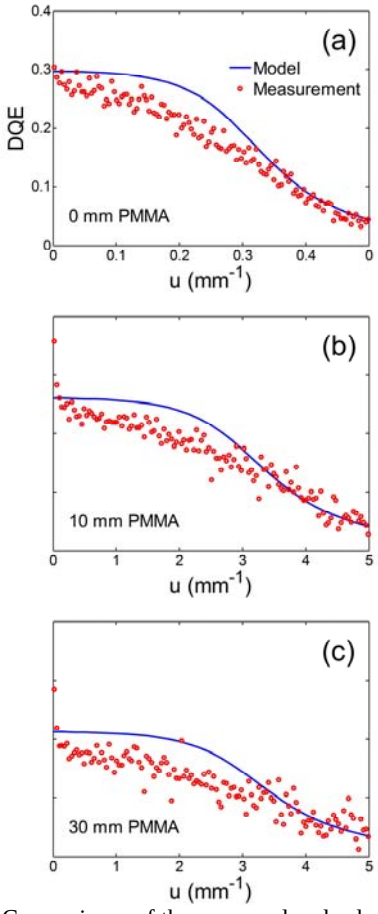

Figure 4. Comparisons of the measured and calculated DQEs for various amounts of scatter.

measurement, the MTF values at the low frequencies drop (LFD), and the amount of this LFD corresponds to the SF. Then, the MTF can be simply described by

$$T_{fit,S}(u) = (1 - SF)T_{fit}(u) \quad (3)$$

The NNPS was determined by using a 2D Fourier analysis of zero-mean images having a size of 512×512 pixels. The zero-mean noise images were obtained by subtracting from each pixel value in the images the mean pixel value and subsequently dividing the subtracted pixel value by the mean pixel value.

3. Preliminary result

Figure 2 shows the MTFs measured for various thicknesses of PMMA. The LFD increased with increasing PMMA thickness, and the amounts of LFD indicated the corresponding SF. The estimated SFs were 0.13, 0.21, and 0.29 for PMMA thicknesses of 10, 20, and 30 mm, respectively. While the solid line describing the measured MTF for PMMA with 0 mm was the result of least-squares of regression fit using Eq. (14), the other lines were simply resulted from the multiplication of the fit result (for PMMA with 0 mm) with the (1-SF) estimated from the LFDs in the measured MTFs. The simple MTF fit models well described the measured results even including the scatter effect. Measurement results of NNPS are shown in Fig. 3. Spectral noise-power densities over the entire frequency range were not much changed with increasing scatter. On the other hand, the calculation results showed that the spectral noise-power densities increased with increasing scatter. This discrepancy may be explained by that the model developed in this study does not account for the changes in x-ray interaction parameters for varying spectral shapes due to beam hardening with increasing PMMA thicknesses. Although some discrepancy between the measurements and calculations, especially at high frequency region, was observed, the model calculations reasonably described the measured NNPS results.

Figure 4 compares the measured and calculated DQE results. As expected, the DQE performance was degraded with increasing scatter. The cascaded DQE model developed in this study reasonably described the measured results.

4. Further study

We will calculate the system DQE with various scatter reduction devices. Using the cascaded model, we investigate the system DQE at typicall scatter condition especially in digital mammography. And it is possible that the system DQE with various SF range and scatter reduction devices can be

expected with this model. It will be performed that we will measure the system DQE with grid to validate the our model.

ACKNOWLEDGMENTS

"This work was supported by the National Research Foundation of Korea (NRF) grant funded by the Korea government (MSIP) (No. 2013M2A2A9046313)."

REFERENCES

[1] S. Yun, J. C. Han, D. W. Kim, H. Youn, H. K. Kim, J. Tanguay, and I. A. Cunningham, "Feasibility of active sandwich detectors for single-shot dual-energy imaging," 2014.

[2] J. C. Han, H. K. Kim, D. W. Kim, S. Yun, H. Youn, S. Kam, J. Tanguay, and I. A. Cunningham, "Single-shot dual-energy x-ray imaging with a flat-panel sandwich detector for preclinical imaging," *Current Applied Physics* **14**(12), pp. 1734–1742, 2014.

[3] L. A. Feldkamp, L. C. Davis, and J. W. Kress, "Practical cone-beam algorithm," *J. Opt. Soc. Am. A* **1**, pp. 612–619, Jun 1984.